Analysis of phase data from ground vibration measurements above a leaking plastic water pipe

O. Scussel[a*], M.J. Brennan[a,b,c], M.K. Iwanaga[b], F.C.L Almeida[c], M. Karimi[d], J.M. Muggleton[a], P.F. Joseph[a], E. Rustighi[e].

[a]Institute of Sound and Vibration Research, University of Southampton, Highfield, SO17 1BJ, Southampton, United Kingdom.

[b]Department of Mechanical Engineering, UNESP-FEIS, Ilha Solteira, São Paulo, 15385-000, Brazil.

[c]Department of Mechanical Engineering, UNESP-FEB, Bauru, São Paulo, 17033-360, Brazil.

[d]Centre for Audio, Acoustics and Vibration, University of Technology Sydney, Sydney, Australia.

[e]Department of Industrial Engineering, University of Trento, Trento, Trentino-Alto Adige, 38121-38123, Italy.

* Corresponding author email: o.scussel@soton.ac.uk

No of pages: 38

No of figures: 13

No of tables: 2

No of references: 29

Revised manuscript submitted to *Journal of Sound and Vibration.*

June 2023.

Abstract

One way to locate a buried plastic water pipe is to measure the surface vibration due to a leak in the region above the pipe, and to process the data to infer the pipe location. This paper investigates the physical mechanisms that propagate leak noise through the pipe and the surrounding soil to the ground surface. An analysis is carried out of the relative phase between vertical ground vibration measurements at points in a grid above the pipe. The study involves experimental measurements from a site in the UK with a more realistic leak mechanism compared to recent research, a simplified analytical model to gain insight into the underlying physics, and a numerical model to validate some of the assumptions made in the derivation of the analytical model. Three waves are principally involved in propagating leak noise to the ground surface from the pipe, namely the predominantly fluid-borne wave in the pipe, and the shear and compressional waves in the soil radiating from the pipe. Their influence on the ground surface vibration is investigated through measured and simulated phase contours over a rectangular grid of surface velocity measurements. It is shown how shear and compressional waves combine to affect the shape of the lines of constant phase on the ground. The results demonstrate the potential of the proposed analytical and numerical models to investigate wave radiation from buried water pipes, and possible pipe location strategies using phase data from surface vibration measurements.

1. Introduction

The need to prevent the wastage of water resources has become increasingly important. The International Energy Agency has estimated that 34% of all water worldwide becomes lost or unaccounted for in the system, referred to as non-revenue water [1]. According to the World Bank, approximately 32 billion cubic meters of water are lost due to leakage globally each year, representing 30-50% of the world's pumped water [2]. The developed world is responsible for half this amount, with leakage in the UK losing approximately 3 billion litres per day. Moreover, a recent report by the BBC suggests that London is among 12 cities at risk of a water crisis and is likely to have supply problems by 2025 and serious shortages by 2040 [3]. Big cities such as Cape Town, Miami, Beijing, Moscow, Mexico City, Cairo and São Paulo are also on this list. To reduce the environmental, social, and economic impacts due to water loss, improved methods for detecting pipe leakage are urgently required [4].

Several technologies and methods for mapping and locating buried pipes have been developed throughout the last century. About 100 years ago Babbit [5] reported leak detection problems in underground pipelines, such as observation of flooded streets, anomalous vegetation growth and the use of methods based on devices as such iron bars, aquaphones (or waterphones) and stethoscope-like apparatus, almost all of which are still familiar in modern approaches to water leak detection. Electromagnetic-based methods such as metal detectors and ground penetrating radar (GPR) have also been widely used due to their non-destructive properties [6]. However, they are far less effective for plastic pipes and for some soil types.

Vibro-Acoustic sensing technologies have some advantages compared to these methods and remain the basis of many water leak detection devices [4]. In recent years, a major UK initiative, entitled "Mapping the Underworld" (MTU) [7], was undertaken to study and develop a range of existing technologies that could be combined into a single device to locate buried pipes infrastructure and cables [8,9]. Leak noise correlators, which use acoustic or vibration

measurements at accessible locations on the pipe (for example, at hydrants) either side of the leak, are effective devices for leak detection that are used world-wide but are limited to relatively short measurement distances from the leak. Alternatives to sensing vibration on a hydrant include measurement of the acoustic pressure inside the pipe with hydrophones, and measurement of the ground surface vibration using geophones, laser vibrometer or accelerometers. Measurements could also be made below the ground surface using a continuous or distributed sensor such as a fiber optic cable [10,11].

A water leak generates noise which propagates along the pipe as a predominantly fluid-borne wave. This wave is the main carrier of leak noise [12,13] and is therefore important in water leak detection and location strategies, such as in the application of correlation techniques in which sensors are placed either along the pipe or on the ground surface. An investigation into the effects of the soil properties on the propagation characteristics of this wave has been reported by Brennan et al. [12]. More recently, Scussel et al. [13] developed a new method for estimating the spectral characteristic of the leak at the source by using sensors attached to the pipe at convenient access points which measured the predominantly fluid-borne wave.

A vibration-based method for locating buried pipes based on the propagation characteristics of the predominantly fluid-borne wave was presented by Muggleton et al. [14] based on the measurement of ground surface responses. The pipe was excited by a shaker which excited this wave, and measurements were made on the ground surface using geophones. The authors found that both magnitude and phase information of the frequency responses between the vibration source and the measured ground responses were important in detecting the buried pipe. Unfortunately, the technique cannot be used in all cases since it requires access to the pipe, which is not always possible.

Some recent models for mapping buried pipes have been developed with different levels of complexity based on image fusion data. Dutta et al. [15] proposed an image fusion

algorithm using a dynamic Bayesian network to process the image data to estimate the most probable pipe location and depth below the surface. The algorithm is based on the combination of three types of image processing: direct excitation image data and ground-excitation image data together with GPR image data. A few years later, Bilal et al. [16] developed a more sophisticated method using a Bayesian mapping model. The sensors included in the experimental apparatus were GPR, Passive Magnetic Field (PMF), vibro-acoustics devices and Low Frequency Electro-Magnetic (LFEM). The data was then processed using machine learning techniques to obtain a real time 3D map to infer the location of the buried pipe. More recently, Yan et al. [17] investigated an imaging fusion technique based on connected graph transversal that provided a better spatial image of the amplitude information to determine the position of the leak source. Experimental results showed that the proposed model gives better magnitude contour plots when image fusion is applied. The authors demonstrated that a suspicious leak area can be identified by extracting and fusing the feature patterns at low frequencies where leak noise dominates.

In addressing the detection and location of buried pipelines there is a lack of analytical modelling of the wave radiation due to a leaking buried pipe capable of encapsulating the key elements of the observed behaviour, yet simple enough to be of general applicability and amenable to straightforward interpretation. Possibly the most complete works found in the literature in this area are by Jette and Parker [18] and Gao et al. [19] which provide the ground surface responses directly above the pipe resulting from radiated conical waves, shear and compressional waves, into the soil. The authors investigated the circumstances in which both shear and compressional waves propagate in the soil from the pipe and how abrupt changes in phase at locations on the surface occur due to wave interaction.

The aim of this paper is to provide experimental, theoretical and numerical investigations into the phase variation of the ground surface velocity due to a buried leaking

plastic pipe. This study can be used to provide valuable guidelines on the effectiveness and design of ground surface velocity measurement techniques for the effective location of leaking pipes. This paper uses the model described in [19] as the starting point, with the aim of deriving approximate expressions for the relative phase of the ground response between positions on the ground surface that are not directly above the pipe. For the sake of simplicity, the model assumes that the pipe is infinitely long and the soil is infinite in all directions. The consequence of this simplification is that the analytical model is valid for the phase distribution over the ground but not for the amplitude, since the infinite soil model does not include the appropriate boundary condition at the ground surface. The predictions from the analytical model are used to interpret the measured phase data from a bespoke pipe test rig for leak detection research [10]. To validate the analytical model for the ground surface phase response, which only involves free rather than forced waves, a novel numerical model is developed. The numerical model also assumes an infinite pipe and an infinite soil medium to significantly reduce the computational burden because the symmetry of the model is maintained.

The paper is organised as follows. Section 2 provides some preliminary experimental data to determine the speed in which leak noise propagates in the pipe, and the frequency bandwidth used for the phase analysis of ground vibration measurements. In Section 3, the analytical model for the ground vibration due to a leak is developed and the numerical model is also presented, where a virtual experiment is conducted using a Finite Element Model (FEM) of the pipe-soil system. In Section 4, analytical, numerical and experimental phase of ground vibration data due to a water leak are compared and discussions of the results are presented. Finally, conclusions are provided in Section 5.

2. Experimental measurements

To obtain some of the parameters used in the analytical and numerical models, experimental data is required and the experimental work is described before the development of the models, which are presented in Section 3. The test rig used in this paper is shown in Fig. 1(a). It is a bespoke test rig installed by South Staffs Water near the Blithfield reservoir in Staffordshire in the UK. The test rig is used by the company to investigate the physical behaviour of buried water pipes when excited by leak noise, and for training purposes [10]. The test-rig consists of a 120 m long, medium-density polyethylene (MDPE) pipe, which has a pipe-wall thickness of 9.8 mm and a mean internal diameter of 160 mm. The pipe is buried at a depth of about 1 m. One end is connected to the water mains which supplies water at an approximate pressure of 6 bar, and the other end is terminated with a blank. The ground surface is grass and the soil in which the pipe is buried, typically found in this region, is a mixture of gravel, sand and clay. A schematic diagram of the test rig shown in Fig. 1(b), which depicts the location of the measurements on the pipe and the ground surface. The figure indicates two hydrants separated 30 m apart and a standpipe connected to one of the hydrants, which is used to generate simulated leak noise by opening a valve. The vibration measurements on the pipe and on the ground surface are now discussed in the following two sections.

2.1 Measurement of pipe vibration

Pipe vibration was measured using two Brüel and Kjaer type 4383 accelerometers. One was attached to the hydrant where the standpipe is connected to the pipe, i.e., the leak position, and the other was attached to the second hydrant 30 m away. These measurements were used to estimate the real and imaginary parts of the wavenumber k related to the predominantly fluid-borne wave in the pipe, and the shear and bulk modulus of the surrounding soil using the procedure described in Scussel et al. [20].

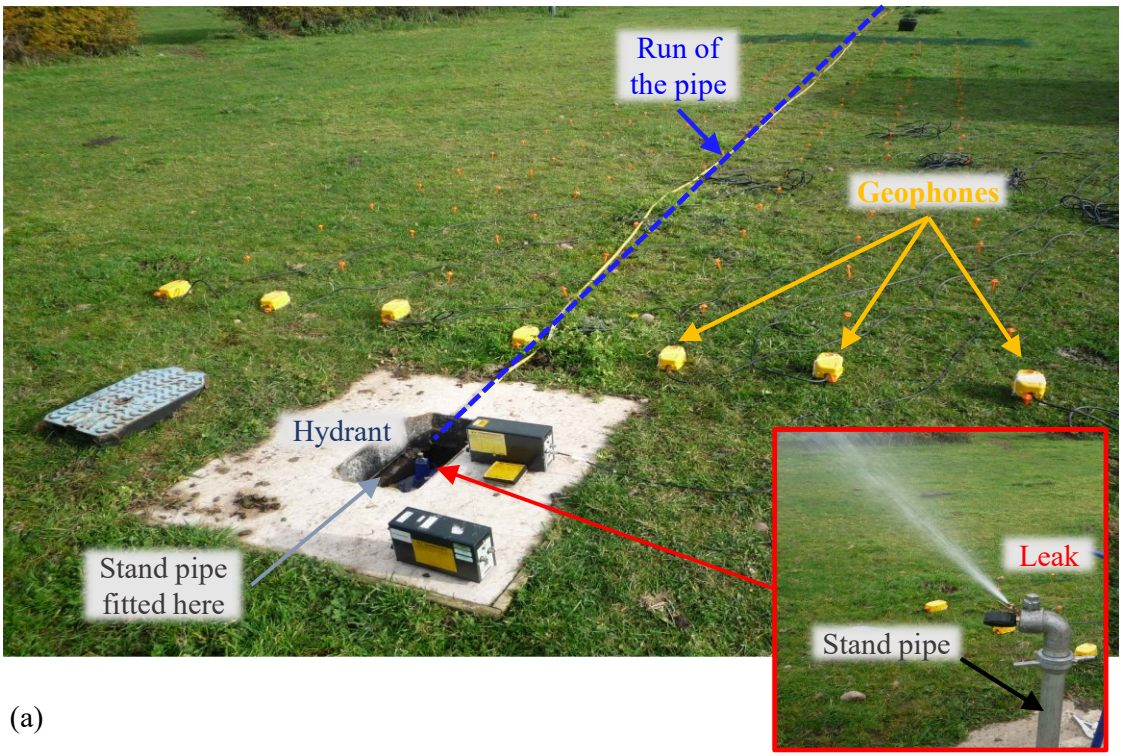

(a)

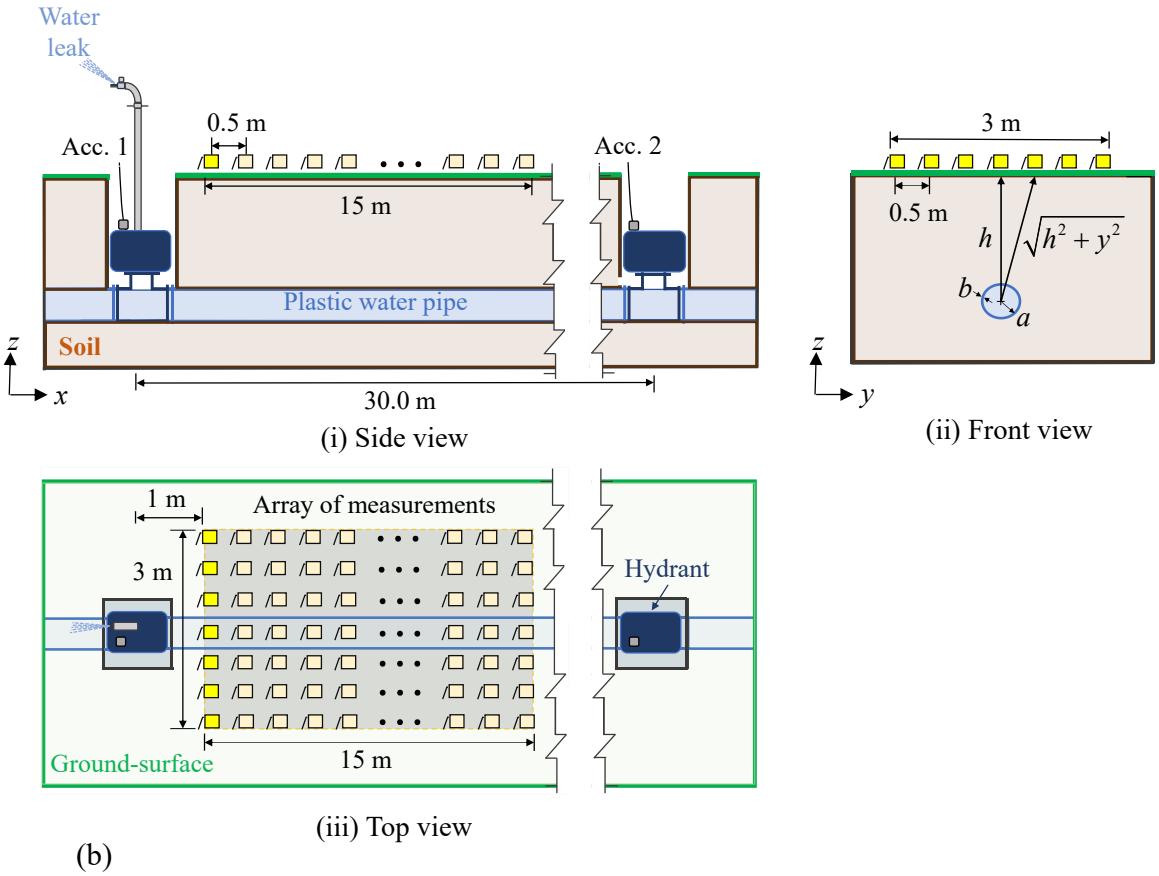

(b)

Figure 1. Typical ground-vibration problem and details of the measurement set-up: (a) Photograph, (b) Schematic diagram of the test rig. In the top view, the grey rectangular array depicts the measurement positions using a column of 7 geophones which were moved over 31

positions in the *x* direction. All the geophone positions were placed on the ground 0.5 m apart in both *x* and *y* directions (not to scale).

To determine *k*, the acceleration transmissibility frequency response function (FRF) *T*, between the 130 s long time histories at Acc. 1 and Acc. 2 shown in Fig. 1(b), is first calculated from the experimental data. The parameters used in the estimation of *T* are a 1024 point-fast Fourier transform with a Hanning window, 128 averages and 50% of window overlap resulting in a frequency resolution of 1 Hz.

Data analysis is confined to a certain frequency bandwidth corresponding to that over which the coherence is above the value of 10^{-3} [14,21,22]. Good coherence is restricted to a specific bandwidth due to the filtering properties of the pipe and the wave attenuation through the soil. This threshold of coherence that depends on the number of averages was found by Muggleton et al. 2011 [14], to represent the lower limit above which the phase of the FRF can be effectively unwrapped.

The measured modulus and phase of the transmissibility FRF as well as the coherence between the accelerations are plotted in Figs. 2(ai-ii) and 2(b) respectively. Also shown in each graph by the light grey area is the frequency bandwidth over which the phase can be unwrapped. This is related to the estimated coherence limits, and is roughly in the range of $30-200$ Hz. The darker grey shaded area shown in each figure depicts the bandwidth $35-75$ Hz related to the ground measurements, which is discussed further in Section 4.

2.1.1 Estimation of the predominantly fluid-borne wavenumber in the pipe

The real and imaginary parts of the wavenumber of the predominantly fluid-borne wave, $\mathrm{Re}\{k\}$ and $\mathrm{Im}\{k\}$ respectively, are calculated from the measured transmissibility FRF T described previously. The complex wavenumber *k* can be determined from the experimental

data by assuming that the fluid-borne wave propagates as a decaying progressive wave without reflection, i.e., $T = e^{-jk\Delta}$, where $\Delta = 30\,\text{m}$, which is the distance between the accelerometers and $j = \sqrt{-1}$. Thus, $\text{Re}\{k\} = -\phi/\Delta$, where ϕ is the phase of *T*, and $\text{Im}\{k\} = \ln|T|/\Delta$ [20]. The real and imaginary parts of *k* are plotted in Figs. 2(ci-ii) respectively. From Fig. 2(ci) it can be seen that the real part of the wavenumber is approximately a straight line as a function of frequency within the bandwidth 50 – 200 Hz, which indicates that the wave is non-dispersive [12], i.e., the wave speed is approximately constant over those range of frequencies.

A straight-line fit to the measured wavenumber estimate is shown in Fig. 2(ci). Noting that $\text{Re}\{k\} = \omega/c_{\text{pipe}}$, where c_{pipe} is the phase velocity (or wave speed) and ω is the angular frequency, then $c_{\text{pipe}} = d\omega/d\left(\text{Re}\{k\}\right)$, which results in a wave speed estimate of approximately 375 m/s.

The imaginary part of the wavenumber is related to the attenuation of the predominantly fluid-borne wave as it propagates along the pipe. To estimate the imaginary part of the wavenumber, a model of the buried water pipe is required. This has been reported in [12,20,23,24] and is described in Appendix A in a compact form. The predicted estimate of $\text{Im}\{k\}$ is plotted in Fig. 2(cii) using the properties of the pipe and soil given in Tabs. 1 and 2. It can be seen that the prediction does not accurately capture the measured wavenumber over the full frequency range of interest, but is reasonably good at predicting the trend of the wave attenuation in the pipe within the frequency range ($35 - 75$ Hz) over which the ground vibration is analysed.

2.2 Measurement of the ground vibration

Fig. 1 depicts the array of I/O SM-24 geophones used to acquire the ground vibration measurements. They were set in a rectangular grid of measurement points, which extended 15 m along the pipe and 1.5 m either side of the pipe.

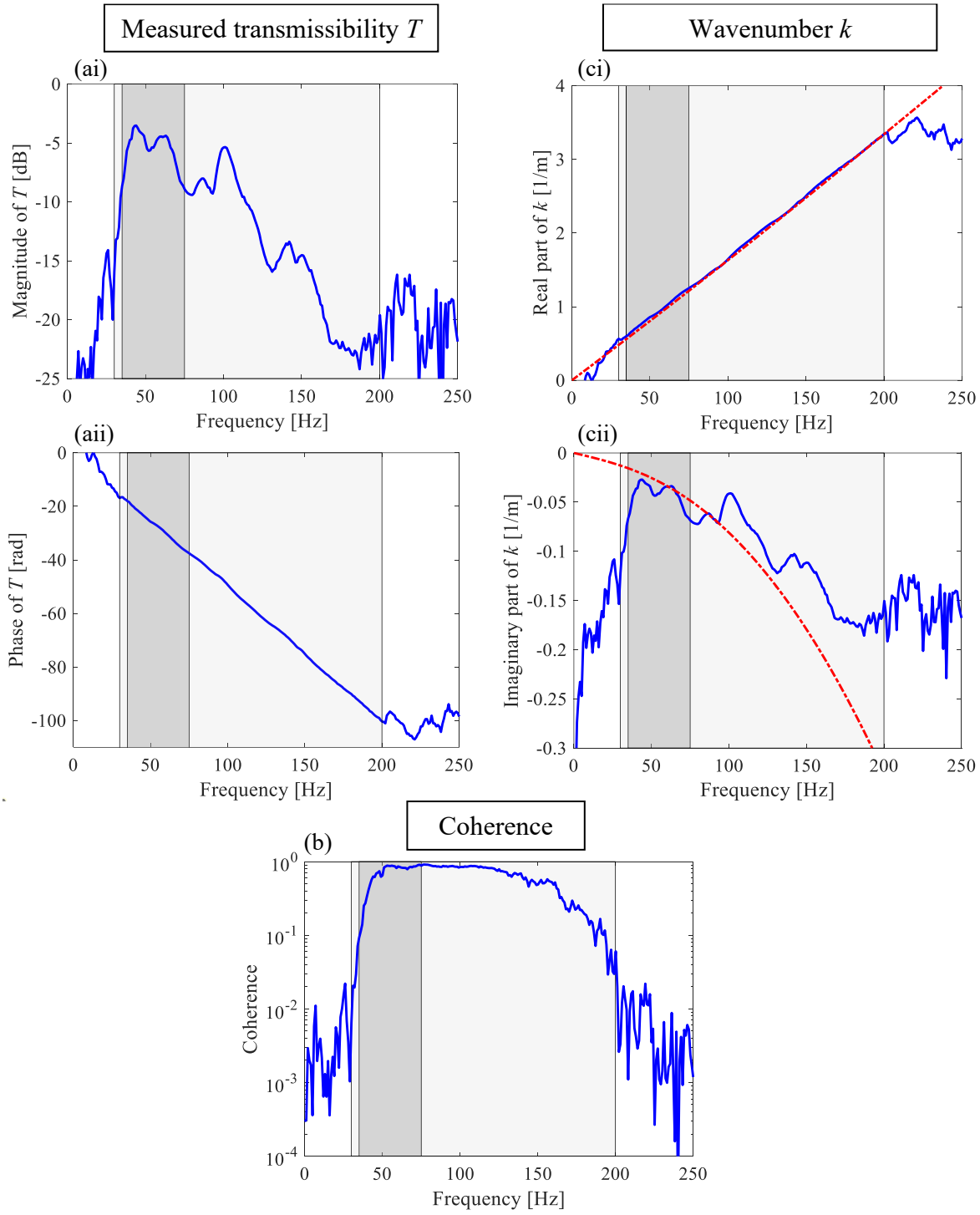

Figure 2. (a) Measured transmissibility T using pipe vibration (Acc. 1 and Acc. 2 depicted in

Fig. 1(b)): (i) Magnitude of T, (ii) Phase of T; (b) Coherence between the accelerations Acc. 1 and Acc. 2; (c) Wavenumber of the predominantly fluid-borne wave using pipe vibration: measured (continuous blue line) and estimated (dash-dotted red line) (i) Real part of k, (ii) Imaginary part of k; The light shaded grey area denotes the frequency range (30-200 Hz) over which the leak noise in the pipe can be detected, traveling at the speed of about 375 m/s. The darker shaded grey area is the frequency range (35-75 Hz) for ground surface vibration analysis.

The grid spacing was 0.5 m, giving a total of 31×7 measurement points. The grid positions (x=0 to 15 m, y=−1.5 m to 1.5 m) are shown in Fig. 1(b), together with the coordinate axes. At each grid point the vertical component of ground vibration was measured, with a leak from the standpipe exciting the system as shown in Fig.1. Seven geophones were used in each measurement, so a single column of grid points (as seen in the top view) could be measured simultaneously, together with the vibration on the pipe next to the standpipe, which acted as a reference signal. The time histories were acquired over 130 seconds with a sampling frequency of 1 kHz. The seven geophones were moved along the pipe to the next grid position and the measurements were repeated. This process was carried out 31 times to produce the full set of 31×7 measurements. As can be seen in Fig. 1, the first column of points was approximately 1 m away from the hydrant to which the standpipe was attached, and the central row of points in the array was located directly above the pipe.

To determine the frequency range over which the analysis of the ground vibration data for the complete grid of measurement points could be reliably performed, the data measured directly above the pipe on the ground surface was first analysed. The unwrapped phase of the cross-power spectral density (CPSD) with respect to the pipe acceleration at the leak position for 31 positions is shown in Fig. 3.

Properties of the plastic water pipe (unit)	Pipe	Water
Young's modulus E_{pipe} (N/m^2)	1.9×10^9	-
Density ρ_{pipe} (kg/m^3)	900	1000
Loss factor η_{pipe}	0.06	-
Poisson's ratio ν_{pipe}	0.4	-
Mean radius a (mm)	80	-
Pipe-wall thickness b (mm)	9.85	-
Wave speed in the pipe c_{pipe} (m/s)	375	-
Bulk modulus of water B_{water} (N/m^2)	-	2.25×10^9
Wave speed in water c_{water} (m/s)	-	1500

Table 1. Geometrical and material properties of the water pipe.

Bulk modulus B_{soil} (N/m^2)	1.28×10^8
Shear modulus G_{soil} (N/m^2)	2.70×10^7
Density ρ_{soil} (kg/m^3)	1850
Compressional wave speed c_d (m/s)	298
Shear wave-speed c_s (m/s)	120
Compressional angle of propagation θ_d ($^\circ$)	40
Shear angle of propagation θ_s ($^\circ$)	72
Burial depth h (m)	1

Table 2. Soil properties.

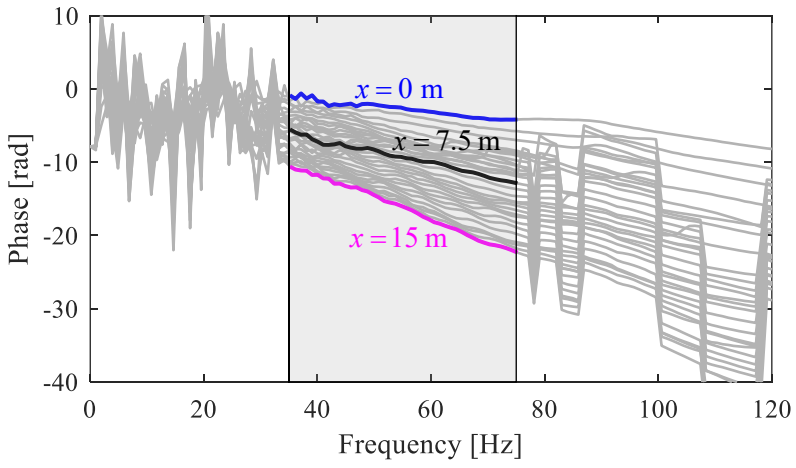

Figure 3. Unwrapped phase of the cross-power spectral density (CPSD) between the acceleration measured at the source position (at the hydrant) and the velocities measured by the geophones on the ground surface at 31 positions right above the pipe: $x = 0$ m (blue line at the top), $x = 7.5$ m (centre black line) and $x = 15$ m (magenta line at the bottom). The shaded

grey region is the frequency bandwidth of 35-75 Hz over which the phase behaviour does not have abrupt discontinuities.

It can be seen that the phase can be unwrapped reasonably well for all the measurement positions in the frequency range $35-75$ Hz. For frequencies below 35 Hz, the data is most likely affected by background noise. Above 75 Hz the leak noise becomes increasingly weaker at measurement positions far from the leak, due to the damping in the system and geometrical spreading of the waves in the soil, leading to poor signal to noise ratios. A comprehensive analysis of the data is presented in Section 4.

3. Estimation of the ground surface vibration due to a leak

To predict the ground surface vibration, two models are developed. One is an analytical model similar to that described for the pipe vibration given in Appendix A. This model is relatively simple, and is limited to predicting only the phase of the waves radiating from the pipe (not including the leak source). The second model is a Finite Element Model (FEM) of the propagation from the pipe to provide a more detailed understanding of the ground vibration on the surface. The FEM is also useful to provide validation data to justify the assumptions made in the analytical model.

3.1 Analytical model

The analytical model used here to understand the phase variation of the ground vibration in the vicinity of the pipe is an extension of the model discussed in Appendix A. The pipe is considered to be infinite in length and buried in an infinite soil medium. The ground surface is assumed to be a horizontal plane above the pipe at a distance h from the centre of the pipe. Thus, reflections are absent from the model. Furthermore, only the phase is predicted without any attempt to predict the amplitude of vibration in the soil.

Depending on the soil properties, a conical shear wave and/or a conical compressional wave may propagate into the soil from the pipe as shown in Figs. 4(ai,ii). Two cones are shown, one for each wave type: a shear wave (inner cone) and compressional wave of higher wave speed (outer cone).

Both shear and compressional waves radiating from the pipe produce a line of constant phase on the surface of the ground, described by a hyperbola intercepting the plane of the ground surface.

The conical wave (for each wave type) will only radiate towards the ground if the speed of the predominantly fluid-borne wave in the pipe (which is responsible for leak noise propagation) exceeds the respective wave speed in the soil, otherwise the wave will be evanescent. This condition is met for typical sandy soil where both compressional and shear waves can radiate from a buried water pipe. However, for a typical stiff clay soil, only a compressional wave radiates. This behaviour has been successfully demonstrated at test sites with different pipe material/geometry and different types of soil in Brazil, Canada and in the UK [12,13,20,21,22]. The wave front of each conical wave has a certain angle of propagation which is determined by the speed of the wave in the soil compared to the wave speed in the pipe. Fig. 4(b) illustrates the wavenumber vector diagrams for each wave type. This diagram shows the relationship between the wavenumber of the predominantly fluid-borne wave in the pipe and the radial outward-going wavenumber component for each wave type in the soil.

In the initial phase of the model development only the vibration directly above the pipe is considered, which is the radial vibration at a distance h from the centre of the pipe.

Referring to Figs. 1 and 4, the vibration at a radial distance $r = h$ is related to the vibration of the pipe surface by [19,25]

$$\mathbf{u}_h = \mathbf{B}_{r=h}\mathbf{B}_{r=a}^{-1}\mathbf{u}_a\,, \tag{1}$$

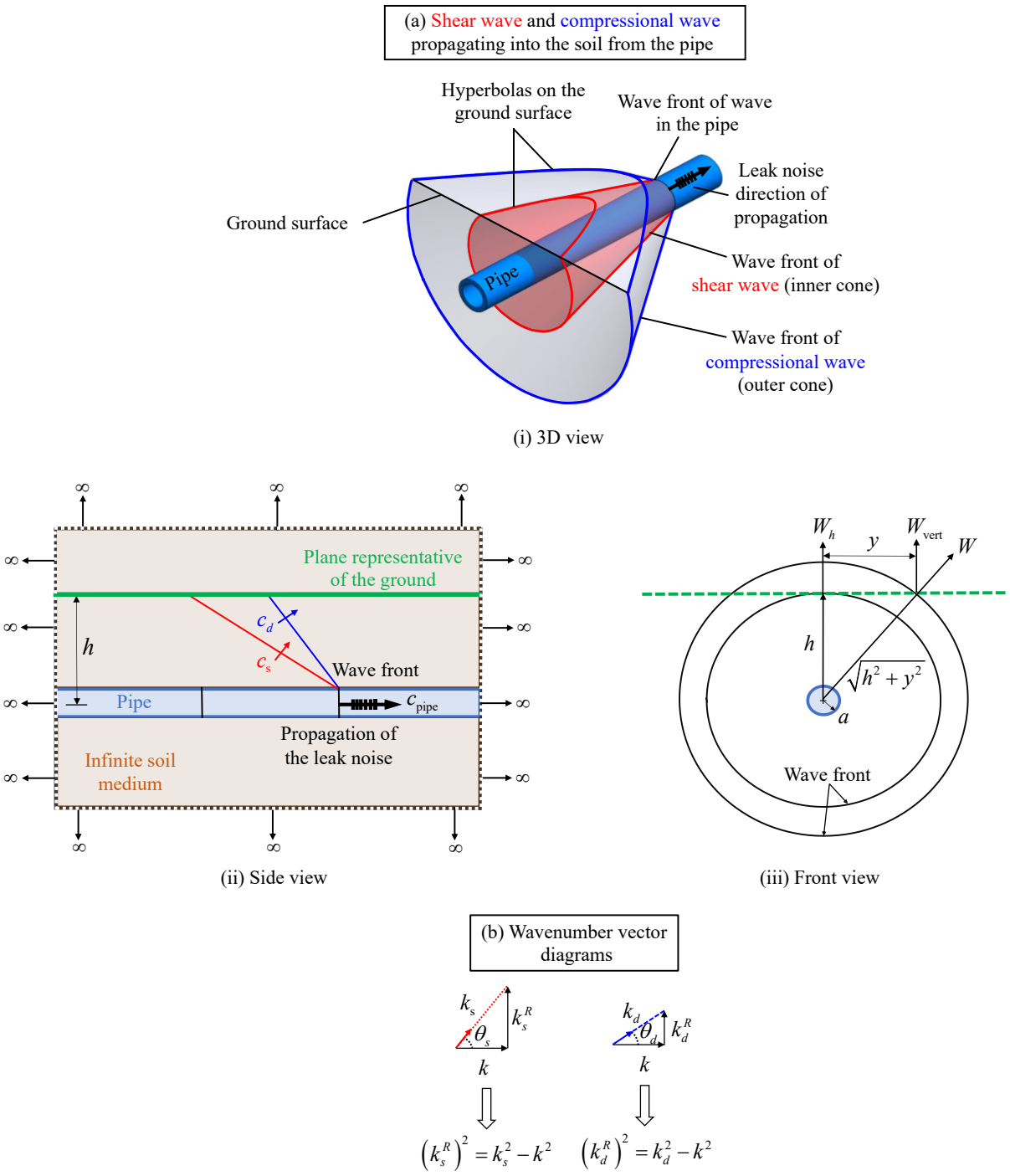

Figure 4. (a) Schematic diagrams showing the body waves propagating into the soil due to the vibration caused by a leak in a buried water pipe: (i) 3D view, (ii) Side view and (iii) Front view. (b) Wavenumber vector diagram showing the relationship between the wavenumber of the shear and compressional waves in the soil with the wavenumber of the predominantly fluid-borne wave in the pipe.

where $\mathbf{B}=\begin{bmatrix} -\mathrm{j}kH_0\left(k_d^R r\right) & k_s^R H_0\left(k_s^R r\right) \\ k_d^R H_0'\left(k_d^R r\right) & -\mathrm{j}kH_0'\left(k_s^R r\right) \end{bmatrix}$ in which $H_0(\bullet)$ is a Hankel function of the second kind of zero order, and $\mathbf{u}_h$ is a velocity vector with axial and vertical components $\mathbf{u}_h=\{U_h \quad W_h\}^T$. From Eq. (A.1) the axial vibration of the pipe is related to the radial vibration by $U_a=\beta W_a$, in which $\beta=-\left(K_{12}^{(\mathrm{pipe})}+K_{12}^{(\mathrm{soil})}\right)/\left(K_{11}^{(\mathrm{pipe})}+K_{11}^{(\mathrm{soil})}\right)$, and from Eq. (A.4) the radial displacement of the pipe W_a is related to the pressure in the pipe P by $W_a/P=1/K^{(\mathrm{water})}\approx\left(k^2/k_{\mathrm{water}}^2-1\right)/\tilde{K}^{(\mathrm{water})}$. Letting $\mathbf{B}_{r=a}^{-1}=\begin{bmatrix} A_{11} & A_{12} \\ A_{21} & A_{22} \end{bmatrix}$, Eq. (1) can be written as

$$\begin{Bmatrix} U_h \\ W_h \end{Bmatrix}=\frac{P}{K^{(\mathrm{water})}}\begin{bmatrix} -\mathrm{j}kH_0\left(k_d^R h\right) & k_s^R H_0\left(k_s^R h\right) \\ k_d^R H_0'\left(k_d^R h\right) & -\mathrm{j}kH_0'\left(k_s^R h\right) \end{bmatrix}\begin{bmatrix} A_{11} & A_{12} \\ A_{21} & A_{22} \end{bmatrix}\begin{Bmatrix} \beta \\ 1 \end{Bmatrix}, \tag{2}$$

The radial displacement W_h may therefore be related to the acoustic pressure inside the pipe P by

$$W_h=\frac{P}{K^{(\mathrm{water})}}\left[k_d^R\left(\beta A_{11}+A_{12}\right)H_0'\left(k_d^R h\right)-\mathrm{j}k\left(\beta A_{21}+A_{22}\right)H_0'\left(k_s^R h\right)\right], \tag{3}$$

At distances sufficiently away from the pipe, such that $\left|k_d^R r\right|>1$ and $\left|k_s^R r\right|>1$, the Hankel functions can be approximated by complex exponential functions [19], resulting in

$$W\left(x,h\right)=W_h e^{-\mathrm{j}kx}=\left(W_h^{(\mathrm{comp})}e^{-\mathrm{j}k_d^R h}+W_h^{(\mathrm{shear})}e^{-\mathrm{j}k_s^R h}\right)e^{-\mathrm{j}\left(kx-\pi/4\right)}, \tag{4}$$

where $W_h^{(\mathrm{comp})}=\dfrac{-\mathrm{j}\left(\beta A_{11}+A_{12}\right)P}{K^{(\mathrm{water})}}\left(\dfrac{2k_d^R}{\pi h}\right)^{1/2}$ and $W_h^{(\mathrm{shear})}=\dfrac{-k\left(\beta A_{21}+A_{22}\right)P}{K^{(\mathrm{water})}}\left(\dfrac{2}{\pi k_s^R h}\right)^{1/2}$ are the complex amplitudes related to the compressional and shear waves respectively. The way in which either the compressional or shear wave propagates into the soil from the pipe can also

be visualised by viewing a cross-section of the pipe-soil system as shown in Fig. 4(aiii). The dashed green line represents the height of the ground surface. It can be seen that a wave front emanating from the pipe first reaches the surface directly above the pipe after travelling a distance *h*, before reaching a point on the ground at a distance *y* from the pipe. The radial displacement is given by

$$W\left(x,\sqrt{y^2+h^2}\right)=\frac{W_h h e^{-\mathrm{j}kx}}{\sqrt{y^2+h^2}}=\left(W_h^{(\mathrm{comp})}e^{-\mathrm{j}k_d^R\sqrt{y^2+h^2}}+W_h^{(\mathrm{shear})}e^{-\mathrm{j}k_s^R\sqrt{y^2+h^2}}\right)\frac{h e^{-\mathrm{j}(kx-\pi/4)}}{\sqrt{y^2+h^2}}. \qquad (5)$$

It should be noted that the radial displacement is the same as the vertical displacement (which is measured) only directly above the pipe, but the phase of the radial displacement is the same as the vertical displacement at any position along the surface, and this quantity is of interest in this paper. One advantage of the simpler analytical model compared to the numerical model (which is described in the next Sub-Section) in the interpretation of the measured data is that the behaviour of the individual waves can be examined individually and contrasted with the situation when both waves propagate simultaneously. To illustrate the behaviour of individual waves, lines of constant phase are estimated for a typical buried plastic water pipe using the nominal properties of the pipe and soil given in Tabs. 1 and 2, corresponding to the pipe system described in Section 2. Figure 5 shows the predicted lines of constant phase at the plane representing the surface for the individual waves, and for the line of constant phase for the combination of the two waves (top view), calculated using Eq. (5) for the two frequencies of 35 Hz (in Fig. 5(a)) and 75 Hz (Fig. 5(b)). Also shown are side views of the buried pipe to illustrate the wave fronts of each wave type to reveal their relationship to the wave front in the pipe. The shear and compressional wave speeds are 120 m/s and 298 m/s, which predicts propagation angles of $\theta_s = 72^{\mathrm{o}}$ and $\theta_d = 40^{\mathrm{o}}$, respectively.

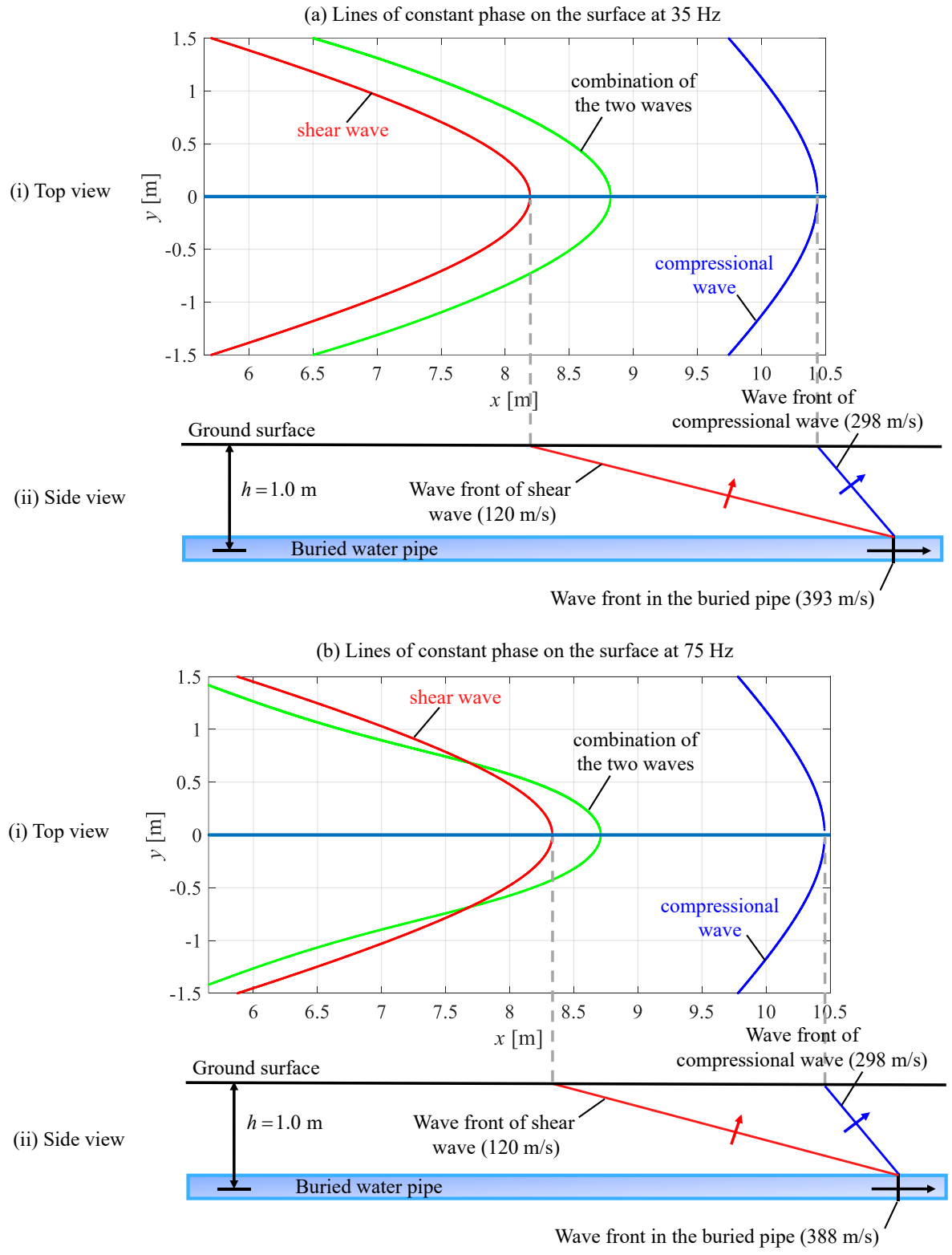

Figure 5. Relationship between the wave fronts predicted on the ground surface and a wave front in the buried pipe at (a) 35 Hz and (b) 75 Hz, (i) Top view and (ii) Side view (not to scale).

The lines of constant phase can be observed to intercept the ground at a horizontal distance of approximately 0.6 m (compressional wave) and 2.7 m (shear wave) away from the wave front in the buried pipe. Fig. 5(a) shows the simulated phase contours above the ground for distances from approximately 5.5 m to 10.5 m. At a frequency of 35 Hz, the combination of the two waves results in a line of constant phase that has similar shape to a hyperbola. However, at a frequency of 75 Hz, the combination of the two waves more closely resembles a bell-like shape. This occurs because of the different amplitudes and phases of the waves at each point on the surface. This feature can also be noted in the numerical and experimental results discussed in Section 4.

3.2 Finite Element Model

A Finite Element Model (FEM) was developed to validate some of the assumptions made in the formulation of the analytical model. As with the analytical model the FEM assumes that the soil and pipe are of infinite extent, but now includes a monopole source to excite the waves in the pipe and in the soil. This has the major advantage of maintaining model symmetry, which means the computational cost is significantly less than it would be if the ground surface was included as this would require a 3D model. The intention is for the numerical model to validate important aspects of the analytical model, such as the propagation of predominantly fluid-borne waves and their radiation into the soil as compressional and shear waves depending upon the soil properties. Neglecting the surface of the soil is justified because the phase, rather than the amplitude of waves reaching the ground surface are of interest. The FEM was developed using the commercial software COMSOL Multiphysics (v5.3). A schematic diagram of the numerical model is shown in Fig. 6. The monopole source was placed 1 m away from the first row of sensors to excite the predominantly fluid-borne wave in the pipe. A perfectly matched layer (PML) was applied on the boundary of the computational domain to simulate infinite media.

A fine mesh of triangular elements was used in the discretisation of the model to ensure the accuracy of the numerical predictions. The water was modelled as a fluid using the COMSOL Pressure Acoustic module. The pipe and soil were modelled as a linear elastic media using the Solid Mechanics module. Full coupling between pipe-wall vibration and the propagation of the predominantly fluid-borne wave in the pipe is included in the FEM.

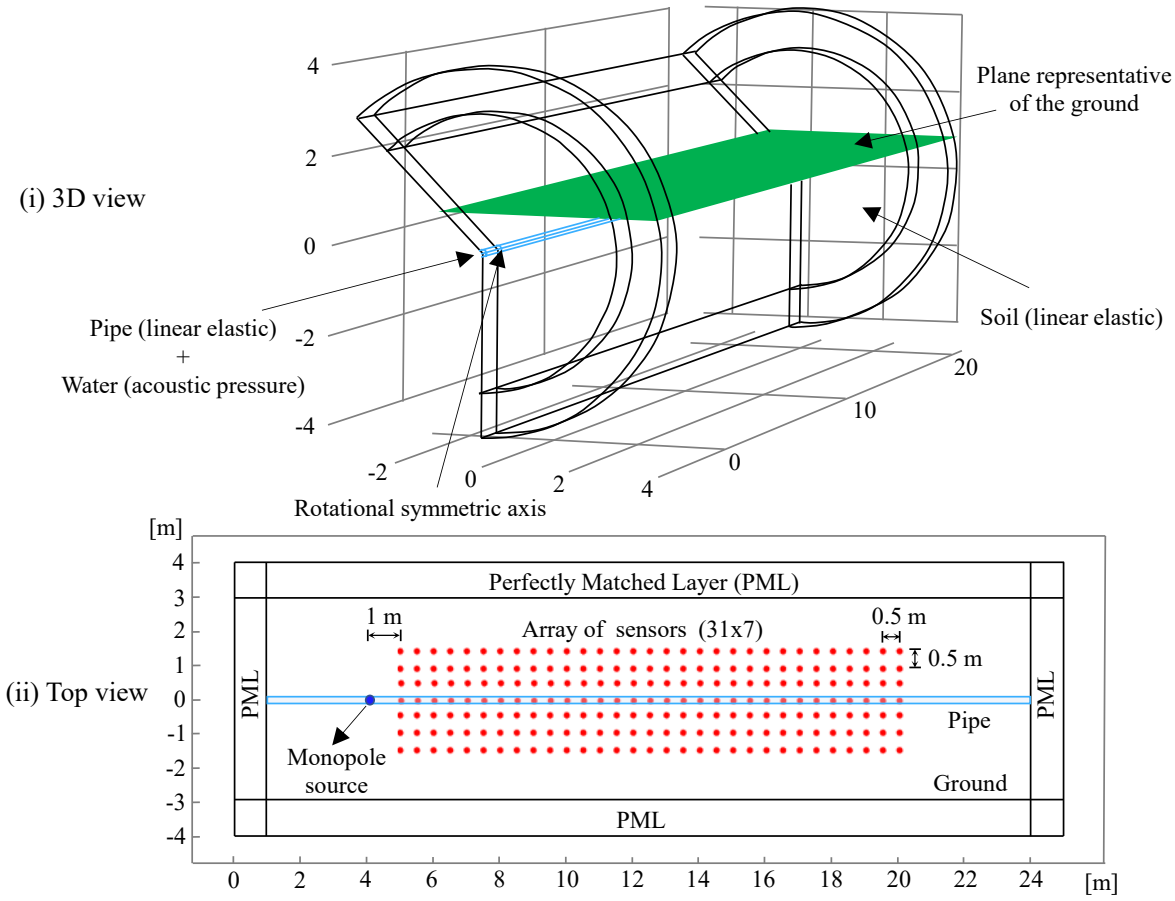

Figure 6. Finite element model of the pipe-soil system simulated in COMSOL.

Vertical velocities at various position on the ground were simulated (in a similar manner as in the Blithfield test rig described in Section 2) over an identical grid to that of the measurements 31x7 points 0.5 m apart (axial and lateral distances) in the plane representative of the ground surface above the plastic water pipe, which is buried at a depth of 1 m, as shown

in Fig. 6. Frequency Response Functions (FRFs) between the monopole source excitation pressure and each vertical velocity were then estimated, over the frequency range $35-75$ Hz.

4. Spatially unwrapped phase of ground vibration data generated by a leak

This Section presents an analysis and comparison between the phase variation of the surface-vibration predicted from the analytical and numerical models, as well as the measured data discussed in Section 2. The two-dimensional phase contours over the ground surface are unwrapped using the algorithm proposed by Herráez et al. [26]. The spatial unwrapping procedure of the phase data was carried out at each frequency over the bandwidth $35-75$ Hz at 1 Hz intervals. The contour plots are lines of constant phase at the surface for each frequency considered. It is not possible to present each plot in figures because of space limitations, however all phase contour plots can be found in an animation provided in the supplementary material. To illustrate the general behaviour, phase responses at the three representative frequencies of 35 Hz, 55 Hz and 75 Hz are plotted in Figs. 7, 8 and 9 respectively. Each figure contains contour plots obtained for (ai) the analytical model, (aii) the numerical model and (aiii) the experimental data. Also shown in each figure, (b) are the unwrapped phases on the surface directly above the pipe for each position x, for the plots in (ai), (aii) and (aiii) respectively. The data in the shaded region, which is at some distance away from the source in the numerical model and experiment, is dominated by the pipe vibration rather than the source and is used to estimate the wave speed. It can be seen that, while there are some differences between the estimated wave speeds calculated from the analytical, numerical and experimental data, it is evident that the wave speed on the ground measured directly above the pipe is similar to that measured using accelerometers on the pipe, which was discussed in Section 2.

Examining the phase contour plot for a frequency of 35 Hz in Fig. 7(ai) predicted by the analytical model, all the contours of constant phase have the same shape, independent of

position. This is because the phase variation over the ground is a superposition of the shear and compressional waves in the soil emanating from the pipe.

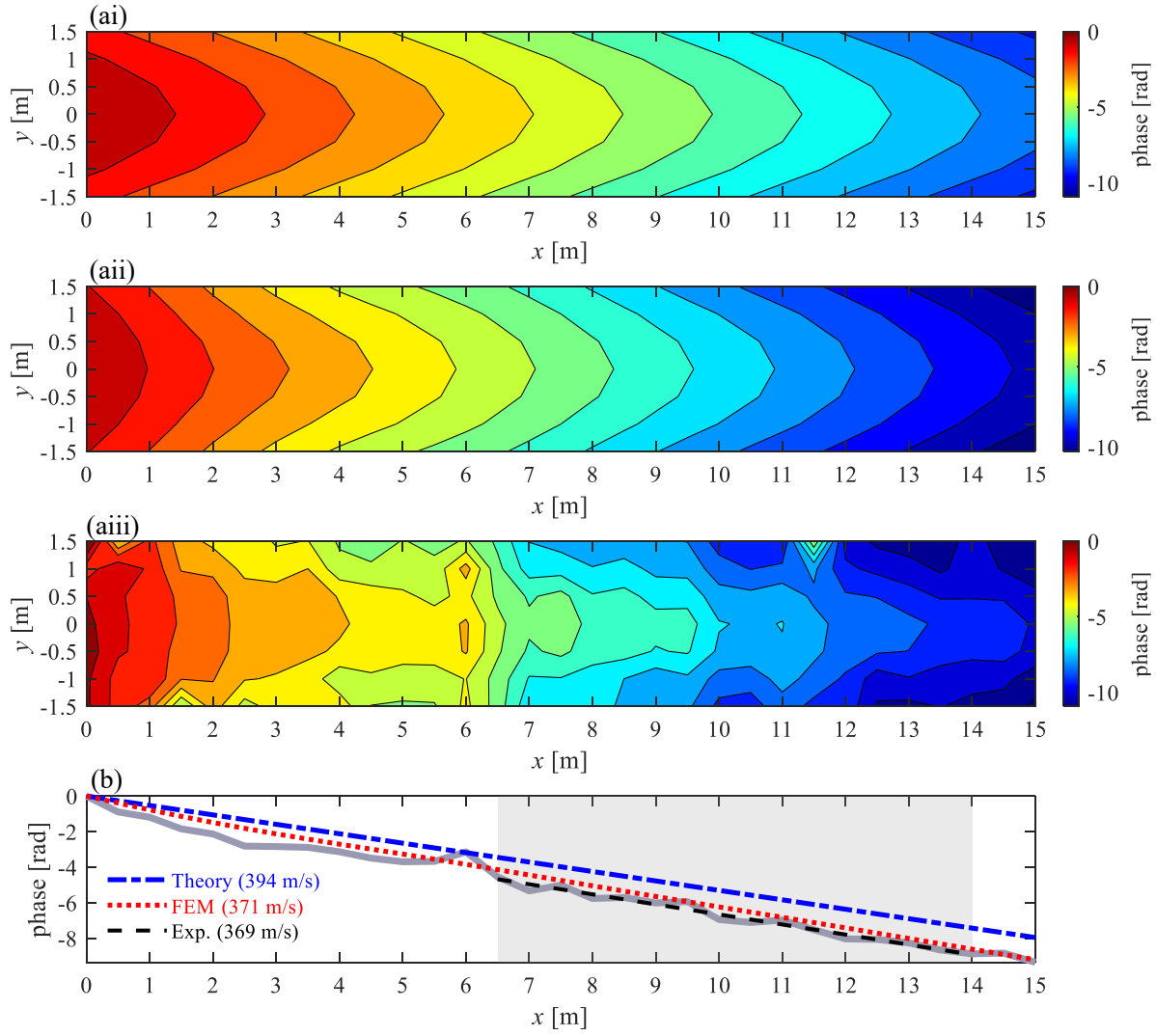

Figure 7. Spatially unwrapped phase at a frequency of 35 Hz: (a) Contour plots for the entire grid of geophones, (i) Theoretical model, (ii) FEM, (iii) Experiment; (b) Phase lines using the geophones right above the pipe showing a comparison between the theory (dotted-dashed blue line), FEM (dotted red line) and the experiment (solid grey line). The grey shaded area represents the region ranging from $x = 6.5$ m to $x = 14$ m and the dashed black line is the linear fit performed on the experimental data over this region.

The shape of each phase contour is similar to a hyperbola, however, as discussed in Section 3, the combination of the two waves results in a shape which is not quite hyperbolic. The phase contours predicted from the numerical model in Fig. 7(aii) can be observed to change shape as the distance from the source increases. This is because close to the monopole source the waves do not radiate from the pipe in the same way as for the infinite pipe assumed in the analytical model. However, from about 5 to 6 m away from the source, the shape of the contours in the numerical model closely resembles those in the analytical model. This suggests that a few metres away from the source, the waves radiating from the pipe dominate the phase behaviour on the surface. The experimental results shown in Fig. 7(aiii) clearly differ from the simulations in Figs. 7(ai) and (aii) in a quantitative sense. Nevertheless, the contours are seen to change shape in the same way as the numerical model, capturing the behaviour both close to and far from the source, thereby providing general validation of the analytical model.

The phase contours shown in Figs. 8 and 9 for frequencies 55 Hz and 75 Hz respectively, are similar to those in Fig. 7. The experimental results in Fig. 8, are particularly clean and show the general behaviour predicted by the analytical and numerical models. Close to the source, it is evident that the source rather than the pipe dominates the phase behaviour, as the contours do not resemble those from waves emanating from an infinite pipe. At distances greater than about 6 metres from the source, the shape of the contours indicates the presence of two waves simultaneously, as discussed previously in Section 3. Deviation in the expected shape of the phase contours, such as that shown at distances of around 11 to 13 m in Fig. 9(aiii), is possibly due to non-homogeneity of the soil.

An alternative view of the phase behaviour on the surface can be seen by removing the phase delay in the direction of the run of the pipe, so that only the phase in the direction orthogonal to the pipe is plotted. This is achieved by considering each line of sensors in the y direction at a given position x, with respect to the sensor directly above the pipe at position x.

The phase plots are shown in Figs. 10, 11 and 12 for frequencies, 35 Hz, 55 Hz and 75 Hz respectively. As with the previous contour plots, each figure contains phase contour plots for (i) the analytical model, (ii) the numerical model and (iii) the experimental data. Also shown in each figure (b) is the phase on the surface for the line of sensors at $x = 7.5$ m.

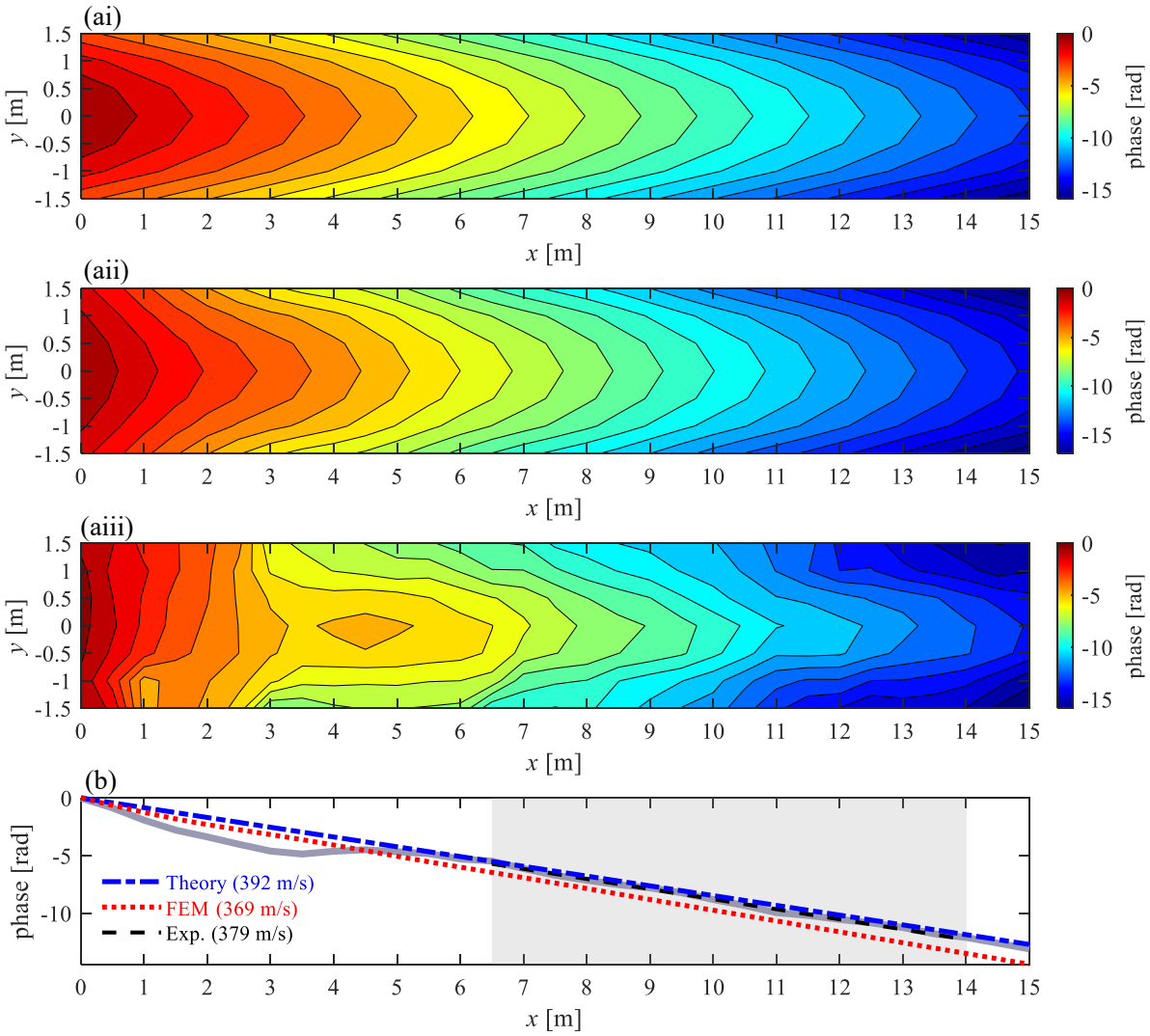

Figure 8. Spatially unwrapped phase at a frequency of 55 Hz: (a) Contour plots for the entire grid of geophones, (i) Theoretical model, (ii) FEM, (iii) Experiment; (b) Phase lines using the geophones right above the pipe showing a comparison between the theory (dotted-dashed blue line), FEM (dotted red line) and the experiment (solid grey line). The grey shaded area represents the region ranging from $x = 6.5$ m to $x = 14$ m and the dashed black line is the linear fit performed on the experimental data over this region.

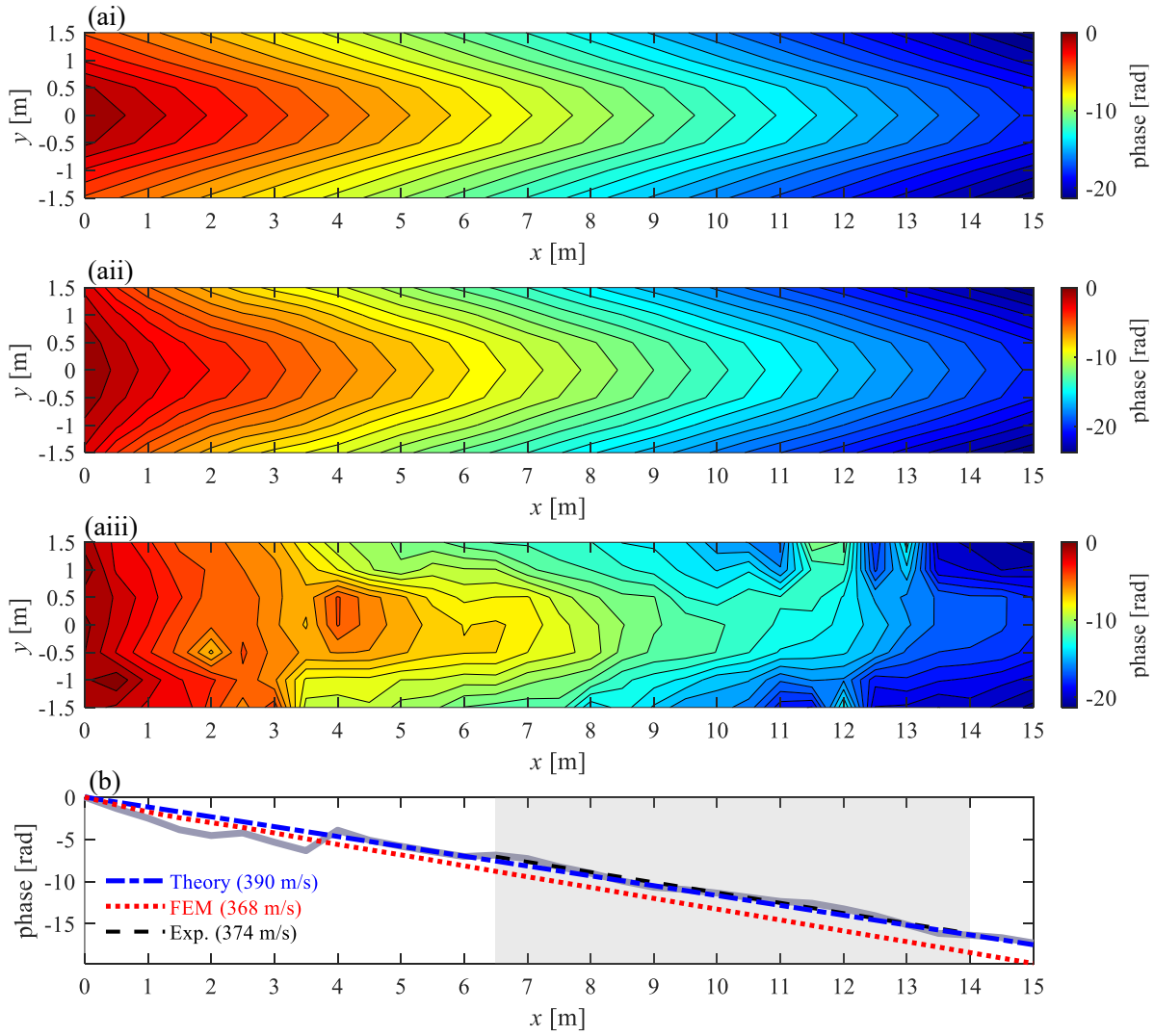

Figure 9. Spatially unwrapped phase at a frequency of 75 Hz: (a) Contour plots for the entire grid of geophones, (i) Theoretical model, (ii) FEM, (iii) Experiment; (b) Phase lines using the geophones right above the pipe showing a comparison between the theory (dotted-dashed blue line), FEM (dotted red line) and the experiment (solid grey line). The grey shaded area represents the region ranging from $x = 6.5$ m to $x = 14$ m and the dashed black line is the linear fit performed on the experimental data over this region.

Note that for a single wave propagating from the pipe, the phase profile shown in (b) would be a hyperbola. In the data presented in the figure it is not possible to see whether or not this is the case, but it is clear that the simulations from the analytical model, the numerical

model and the experimental data are qualitatively similar. As with the contour plots discussed previously the full set of data can be seen in the animation presented as supplementary material.

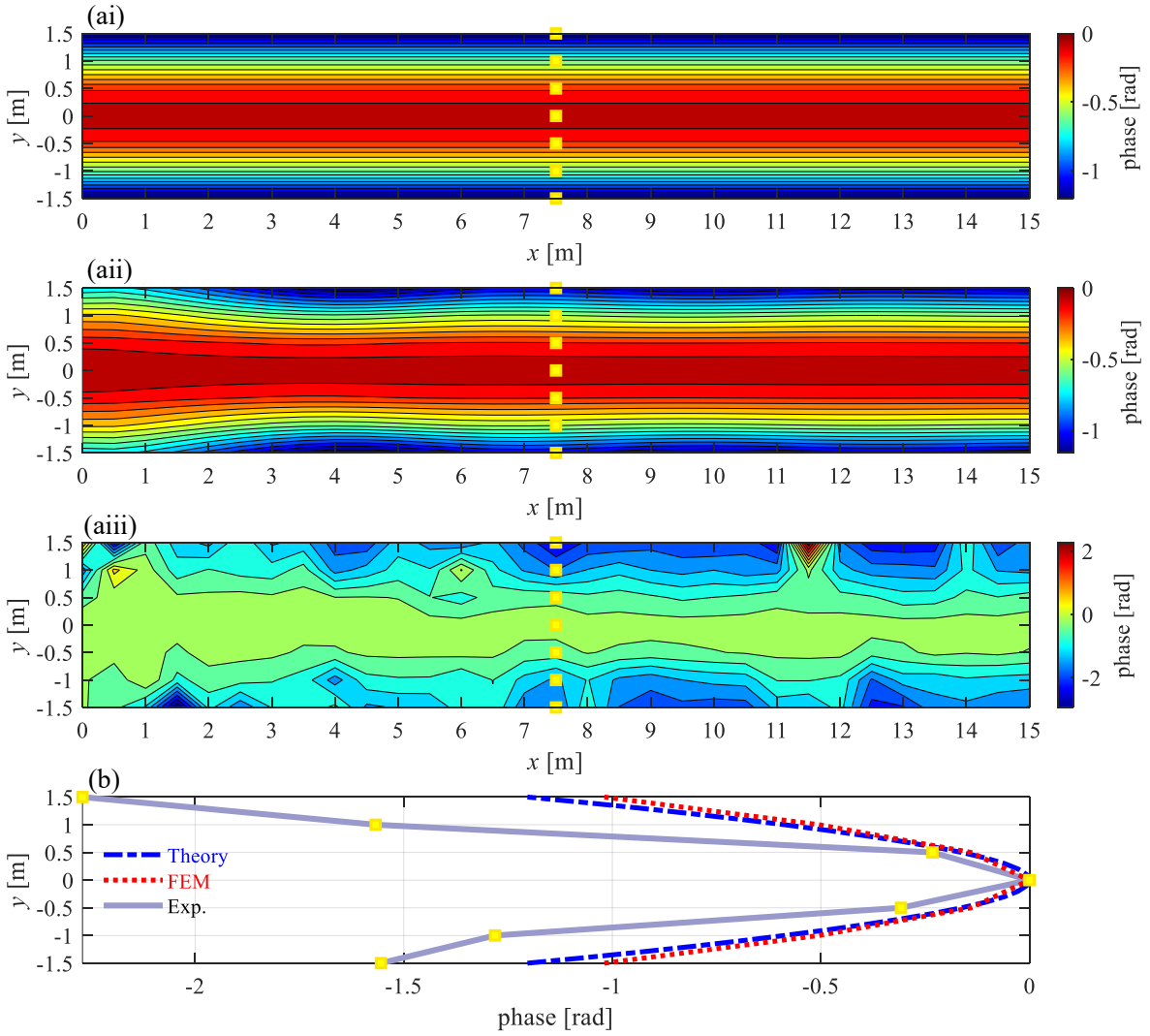

Figure 10. Spatially unwrapped phase at a frequency of 35 Hz: (a) Contour plots for the entire grid of geophones normalized by the phase right above the pipe, (i) Theoretical model, (ii) FEM, (iii) Experiment; (b) Phase lines using the geophones across the pipe located at $x = 7.5$ m showing a comparison between the theory (dotted-dashed blue line), FEM (dotted red line) and the experiment (solid grey line).

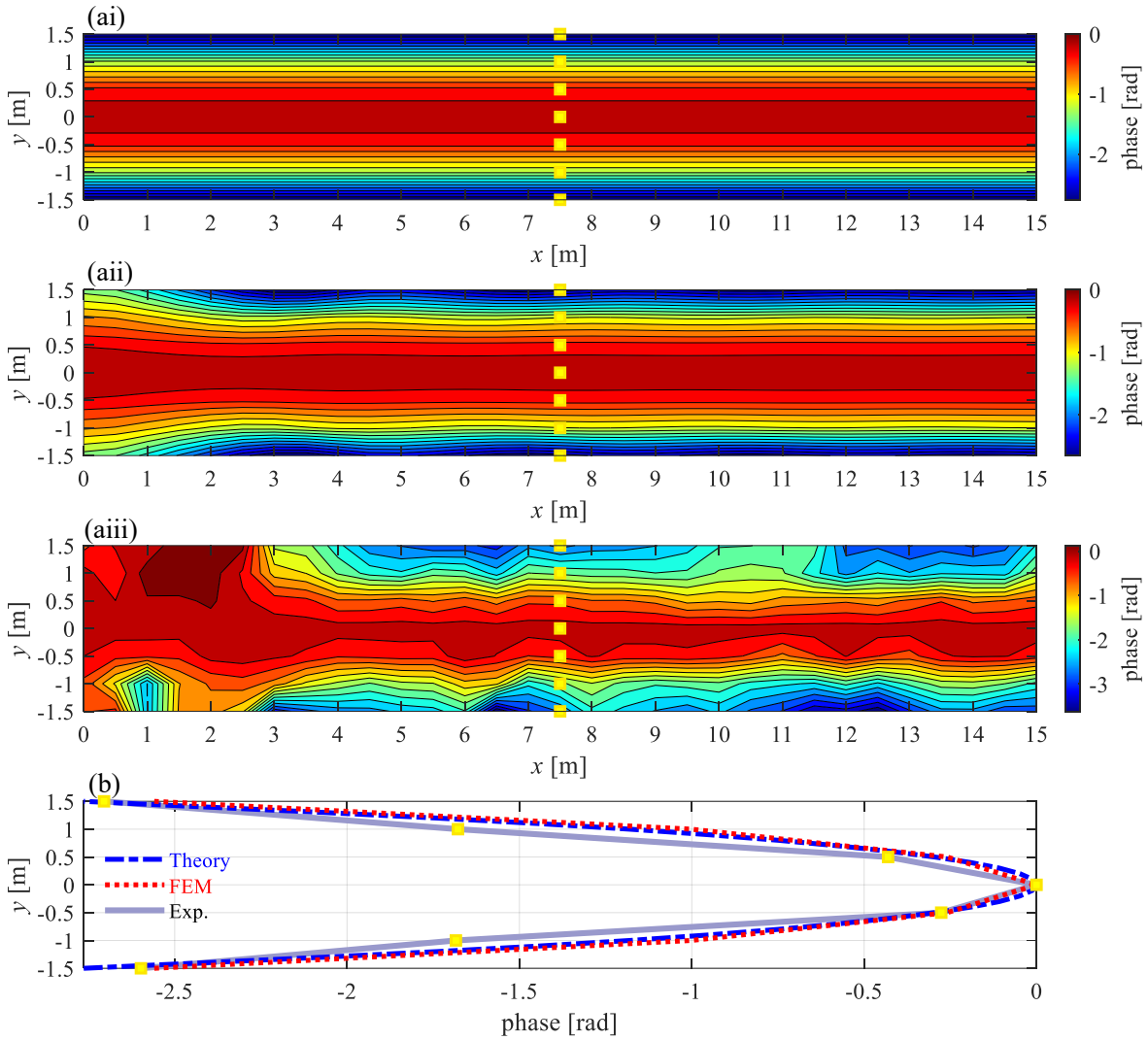

Figure 11. Spatially unwrapped phase at a frequency of 55 Hz: (a) Contour plots for the entire grid of geophones normalized by the phase right above the pipe, (i) Theoretical model, (ii) FEM, (iii) Experiment; (b) Phase lines using the geophones across the pipe located at $x = 7.5$ m showing a comparison between the theory (dotted-dashed blue line), FEM (dotted red line) and the experiment (solid grey line).

Examination of the phase plots in Figs. 10, 11 and 12 clearly reveal the run of the pipe, especially at the frequencies of 35 Hz and 55 Hz. For the experimental results, the pipe location is not quite evident at all frequencies and at some locations but, taken as a whole, the evidence

is compelling, suggesting that phase mapping of surface vibration data could be a useful tool in determining the location of a buried plastic water pipe excited by a leak.

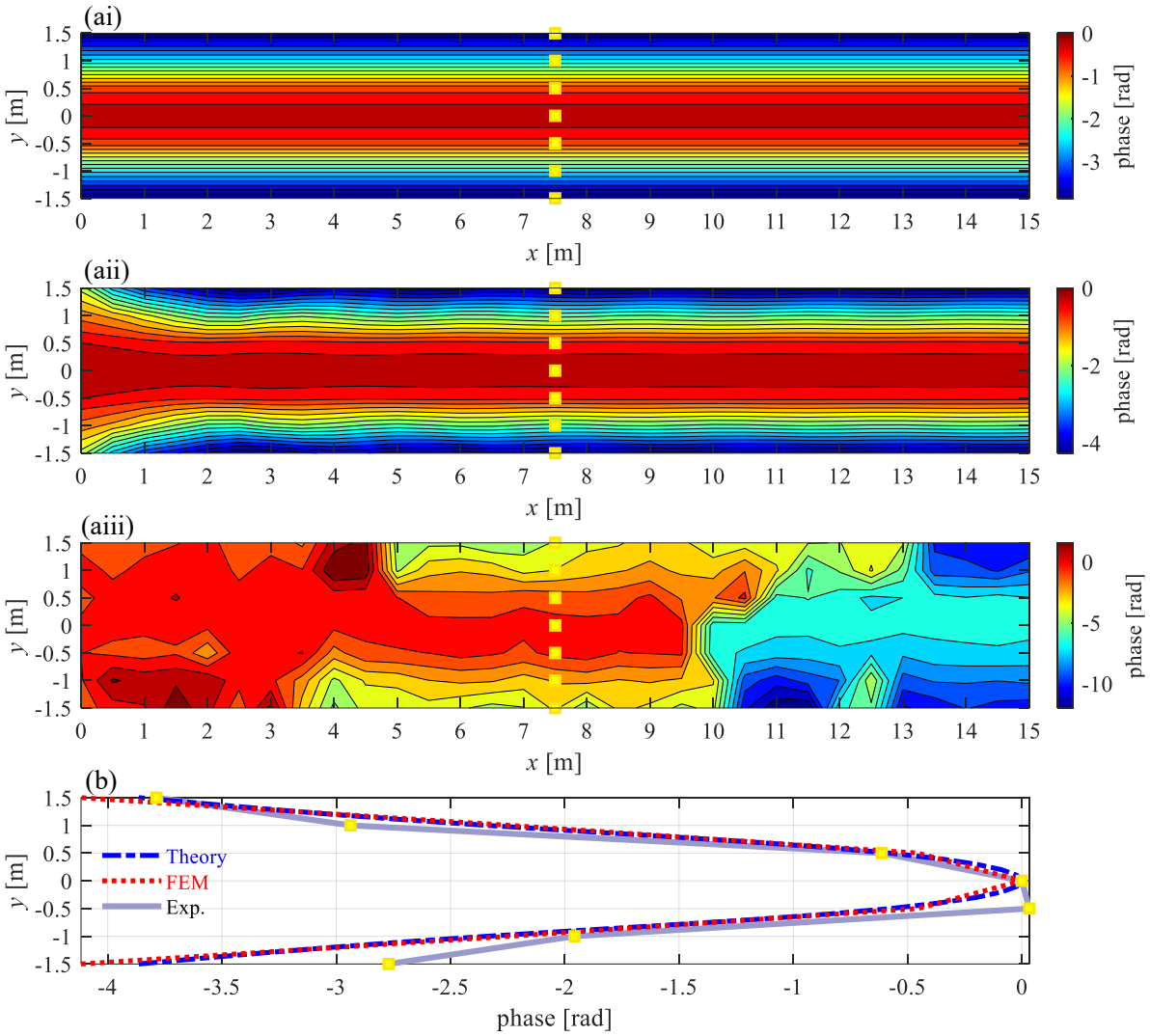

Figure 12. Spatially unwrapped phase at a frequency of 75 Hz: (a) Contour plots for the entire grid of geophones normalized by the phase right above the pipe, (i) Theoretical model, (ii) FEM, (iii) Experiment; (b) Phase lines using the geophones across the pipe (located at $x = 7.5$ m showing a comparison between the theory (dotted-dashed blue line), FEM (dotted red line) and the experiment (solid grey line).

5. Conclusions

In this paper, phase data on the ground surface above a leaking buried plastic water pipe has been examined. To help understand the behaviour of measured data, two approaches were taken. The first is a simplified analytical model, and the other is a numerical approach using a commercial finite element package. In both of these approaches, the pipe and the surrounding soil were assumed to be of infinite extent since no attempt was made to model the ground surface.

In the analytical model the individual effects of shear and compressional waves emanating from the pipe into the soil on the phase contours measured from a sensor array on a plane representative of the ground surface were studied. Predictions from the model enables the shape of the phase contours in the experimental data to be interpreted. A fundamental assumption in this model, for the pipe material and geometry studied, is the presence of a predominantly fluid-borne wave in the pipe, causing radial motion of the pipe, which generates shear and compressional waves that propagate towards surface. The numerical model was also investigated, for the two main reasons: (i) to provide validation data for the analytical model and, (ii) to allow the inclusion of acoustic excitation sources, which created different phase contours close to the excitation position compared to those far from the source. This additional information also helped in the interpretation of the measured phase data on the surface. In general, the simulations show good qualitative agreement with measurements from a test rig in which an array of geophones was used to measure ground vibration due to a leak from a buried plastic water pipe. However, at some frequencies and at some locations, the measurements clearly did not follow the predicted phase behaviour, and this is probably due to non-homogeneity of the soil. The results from the study in this paper suggest that phase analysis of surface vibration data could be a useful way to determine the location of a buried water pipe that is generating noise due to a leak.

Acknowledgments

The authors gratefully acknowledge the financial support provided by Engineering and Physical Sciences Research Council (EPSRC) under RAINDROP project (EP/V028111/1), the São Paulo Research Foundation (FAPESP) under Grant numbers 2018/25360-3 and 2020/12251-1, and the Coordination for the Improvement of Higher Education Personnel (CAPES) under Grant numbers 432272/2018-6 and 88887.374001/2019-00. The authors also would like to thank the Brazilian water and waste management company (Sabesp) for partly funding this work.

References

[1] https://www.fluencecorp.com/what-is-non-revenue-water/ (access on 20 Jan. 2023).

[2] https://blogs.worldbank.org/water/what-non-revenue-water-how-can-we-reduce-it-better-water-service (access on 20 Jan. 2023).

[3] https://www.bbc.com/news/world-42982959 (access on 20 Jan. 2023).

[4] Y. Liu; D. Habibi, D. Chai, X. Wang, H. Chen, Y. Gao, S. Li. A Comprehensive Review of Acoustic Methods for Locating Underground Pipelines. Appl. Sci 10(3) (2020) 1031, https://doi.org/10.3390/app10031031

[5] H.E. Babbitt, 1920. The detection of leaks in underground pipes. Journal of AWWA 7 (1920) 589-595, https://www.jstor.org/stable/41224698

[6] Q. Wu, X. Zhou and H. Chen. Underground Pipeline Mapping Based on Dirichlet Process Mixture Model, in IEEE Access 8 (2020) 118114-118124, https://doi.org/10.1109/ACCESS.2020.3005420

[7] Mapping the Underworld, 2021. http://www.mappingtheunderworld.ac.uk/ (access on 20 Jan. 2023).

[8] J.M. Muggleton, E. Rustighi. Mapping the Underworld: recent developments in vibro-acoustic techniques to locate buried infrastructure, Geotech. Lett. 3(3) (2013) 137-141, https://doi.org/10.1680/geolett.13.00032

[9] C.D.F. Rogers, T. Hao, S.B. Costello, M.P.N. Burrow, N. Metje, D.N. Chapman, J. Parker, R.J. Armitage, J.H. Anspach, J.M. Muggleton, K.Y. Foo, P. Wang, S.R. Pennock, P.R. Atkins, S.G. Swingler, A.G. Cohn, K. Goddard, P.L. Lewin, G. Orlando, M.A. Redfern, A.C.D. Royal, A.J. Saul. Condition assessment of the surface and buried infrastructure – A proposal for integration, Tunn. Undergr. Space Technol. 28 (2012) 202-211, https://doi.org/10.1016/j.tust.2011.10.012

[10] A.C.D. Royal, P.R. Atkins, M.J. Brennan, D.N. Chapman, H. Chen, A.G. Cohn, K.Y. Foo, K.F. Goddard, R. Hayes, T. Hao, P.L. Lewin, N. Metje, J. M. Muggleton, A. Naji, G. Orlando, S.R. Pennock, M.A. Redfern, A.J. Saul, S.G. Swingler, P. Wang and C.D.F Rogers. Site assessment of multiple-sensor approaches for buried utility detection. Int. J. Geophsy. (2011) Article ID 496123, https://doi.org/10.1155/2011/496123

[11] J. Jiang, F. Liu, H. Wang, S. Li, W. Gan, R. Jiang. Lateral positioning of vibration source for underground pipeline monitoring based on ultra-weak fibre Bragg grating sensing array, Measurement 172 (2021) 108892, https://doi.org/10.1016/j.measurement.2020.108892

[12] M.J. Brennan, M. Karimi, J.M. Muggleton, F.C.L de Almeida, F. K. de Lima, P.C. Ayala, D. Obata, A.T. Paschoalini, N. Kessissoglou. On the effects of soil properties on leak noise propagation in plastic water distribution pipes, J. Sound Vib. 427 (2018) 120-133, https://doi.org/10.1016/j.jsv.2018.03.027

[13] O. Scussel, M.J. Brennan, F.C.L. Almeida, J.M. Muggleton, E. Rustighi, P.F. Joseph. Estimating the spectrum of leak noise in buried plastic water distribution pipes using acoustic or vibration measurements remote from the leak, Mech. Syst. Signal Process. 147 (2021) Article 107059, https://doi.org/10.1016/j.ymssp.2020.107059

[14] J.M. Muggleton, M.J. Brennan, Y. Gao. Determining the location of buried plastic water pipes from measurements of ground surface vibration, J. Appl. Geophys. 75(1) (2011) 54-61, https://doi.org/10.1016/j.jappgeo.2011.06.030

[15] R. Dutta, A. G. Cohn, J.M. Muggleton. 3D mapping of buried underworld infrastructure using dynamic Bayesian network based multi-sensory image data fusion, J. Appl. Geophys. 92 (2013) 8-9, http://dx.doi.org/10.1016/j.jappgeo.2013.02.005

[16] M. Bilal, W. Khan, J.M. Muggleton, E. Rustighi, H. Jenks, S. R. Pennock, P. R. Atkins, A. Cohn. Inferring the most probable maps of underground utilities using Bayesian mapping model, J. Appl. Geophys. 150 (2018) 52-66, https://doi.org/10.1016/j.jappgeo.2018.01.006

[17] S. Yan, H. Yuan, Y. Gao, B. Jin, J.M. Muggleton, L. Deng. On Image Fusion of Ground Surface Vibration for Mapping and Locating Underground Pipeline Leakage: An Experimental Investigation. Sensors 20 (2020) 1896, https://doi.org/10.3390/s20071896

[18] A.N. Jette, J.G. Parker. Surface displacements accompanying the propagation of acoustic waves within an underground pipe. J. Sound Vib, 69(2) (1980) 265-274, https://doi.org/10.1016/0022-460X(80)90611-2

[19] Y. Gao, J.M. Muggleton,, Y. Liu, E. Rustighi. An analytical model of ground surface vibration due to axisymmetric wave motion in buried fluid-filled pipes. J. Sound Vib. 395 (2017) 142–159, https://doi.org/10.1016/j.jsv.2017.02.022

[20] O. Scussel, M.J. Brennan, J.M. Muggleton, F.C.L. Almeida, A. T. Paschoalini, Estimation of the bulk and shear moduli of soil surrounding a plastic water pipe using measurements of the predominantly fluid wave in the pipe, J. Appl. Geophys., 164 (2019), pp. 237–246, https://doi.org/10.1016/j.jappgeo.2019.01.010

[21] F.C.L. Almeida, M.J. Brennan, P.F. Joseph, S. Whitfield, S. Dray. On the acoustic filtering of the pipe and sensor in a buried plastic water pipe and its effect on leak detection: an

experimental investigation, Sensors 14(3) (2014), 5595-5610, https://doi.org/10.3390/s140305595

[22] F.C.L. Almeida, M.J. Brennan, P.F. Joseph, S. Dray, S. Whitfield, A.T. Paschoalini. Towards in-situ measurement of wave velocity in buried plastic water distribution pipes for the purposes of leak location, J. Sound Vib. 359 (2015) 40-55, https://doi.org/10.1016/j.jsv.2015.06.015

[23] Muggleton, J.M., Brennan, M.J., Linford, P.W. Axisymmetric wave propagation in fluid-filled pipes: wavenumber measurements in in vacuo and buried pipes. J. Sound Vib. vol 270 (2004), pp. 171–190. https://doi.org/10.1016/S0022-460X(03)00489-9.

[24] Y. Gao, Y. Liu, J.M. Muggleton, Axisymmetric fluid-dominated wave in fluid-filled plastic pipes: Loading effects of surrounding elastic medium, Appl. Acoust. 116 (2017) 43-49. http://dx.doi.org/10.1016/j.apacoust.2016.09.016

[25] J.M. Muggleton, O. Scussel, E. Rustighi, M.J. Brennan, F.C.L. Almeida, M. Karimi, P.F. Joseph (2023). A Simplified Model of the Ground Surface Vibration Arising from a Leaking Pipe. In: Dimitrovová, Z., Biswas, P., Gonçalves, R., Silva, T. (eds) Recent Trends in Wave Mechanics and Vibrations. WMVC 2022. Mechanisms and Machine Science, vol 125. Springer, Cham. https://doi.org/10.1007/978-3-031-15758-5_105

[26] M.A Herráez, D.R. Burton, M.J. Lalor, M.A. Gdeisat. Fast two-dimensional phase-unwrapping algorithm based on sorting by reliability following a noncontinuous path. App. Opt. 41(35) (2002) 7437-7444, https://doi.org/10.1364/AO.41.007437

[27] Fahy F, Gardonio P, Sound and structural vibration, second ed., Elsevier, 2007.

[28] M.K. Iwanaga, M.J. Brennan, F.C.L. Almeida, O. Scussel, S.O. Cezar, A laboratory-based leak noise simulator for buried water pipes, Appl. Acoust. 185 (2022) 108346. https://doi.org/10.1016/j.apacoust.2021.108346

[29] O. Scussel, M.J. Brennan, F.C.L. Almeida, M.K. Iwanaga, J.M. Muggleton, P.F. Joseph, Y. Gao. Key Factors That Influence the Frequency Range of Measured Leak Noise in Buried Plastic Water Pipes: Theory and Experiment. Acoustics 5 (2023) 490-508, https://doi.org/10.3390/acoustics5020029

Appendix A. Model for the predominantly fluid-borne wavenumber in the buried pipe

A schematic diagram of the buried pipe system (excluding the hydrants), which includes the pipe-wall, the water in the pipe and the surrounding soil is shown in Fig. A.1. It has a mean radius a and wall-thickness b.

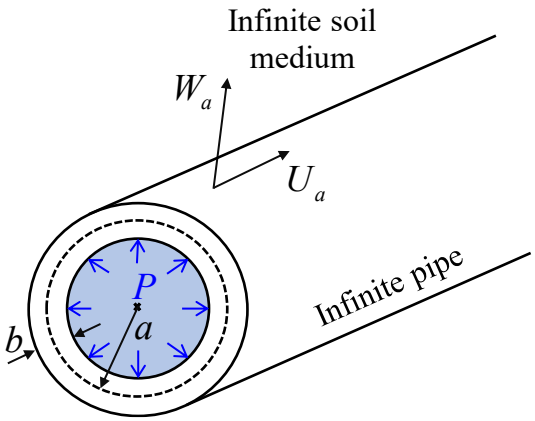

Figure A1. Schematic diagram of the buried pipe showing the pipe geometry, radial and axial displacements of the pipe and the pressure within the fluid.

In the derivation of the analytical model, the following simplifying assumptions are made:

- The pipe and soil are of infinite extent in the axial direction, and the soil is of infinite extent in the radial direction.
- The predominantly fluid-borne axisymmetric wave is the predominant wave propagating in the pipe and is responsible for the propagation of leak noise.
- Shear and compressional waves can propagate in the soil.

- The frequency range of interest is well below the pipe ring frequency, so that bending in the pipe-wall is neglected.
- The frequency range of interest is such that an acoustic wavelength of water is much greater than the diameter of the pipe.
- The multiple internal reflections of the predominantly fluid-borne axisymmetric wave due to discontinuities are neglected for simplicity.

The analytical model, which is based on that described by Gao et al. [24], uses the concept of wave dynamic stiffness K which is similar to wave impedance described by Fahy and Gardonio [27], but rather than using the variables of force (or pressure) and velocity, displacement is used instead of velocity, as this is more convenient. The dynamics of the pipe-soil system can be described by [28,29]

$$\left[\mathbf{K}^{(\text{pipe})}+\mathbf{K}^{(\text{water})}+\mathbf{K}^{(\text{soil})}\right]\mathbf{u}_a=\mathbf{0}, \tag{A.1}$$

where $\mathbf{u}_a=\left\{U_a \quad W_a\right\}^T$, in which the superscript T denotes the transpose, and

$$\mathbf{K}^{(\text{pipe})}=\begin{bmatrix}K_{11}^{(\text{pipe})} & K_{12}^{(\text{pipe})}\\ K_{21}^{(\text{pipe})} & K_{22}^{(\text{pipe})}\end{bmatrix}=\begin{bmatrix}(ka)^2\,\tilde{K}^{(\text{pipe})}-\omega^2\rho_{\text{pipe}}b & \mathrm{j}\nu_{\text{pipe}}(ka)\tilde{K}^{(\text{pipe})}\\ -\mathrm{j}\nu_{\text{pipe}}(ka)\tilde{K}^{(\text{pipe})} & \tilde{K}^{(\text{pipe})}-\omega^2\rho_{\text{pipe}}b\end{bmatrix}, \tag{A.2}$$

in which $\mathbf{K}^{(\text{pipe})}$ is the wave dynamic stiffness matrix for the pipe-wall, where $\tilde{K}^{(\text{pipe})}=E_{\text{pipe}}^{*}b\Big/\left[a^2\left(1-\nu_{\text{pipe}}^2\right)\right]$, in which $E_{\text{pipe}}^{*}=E_{\text{pipe}}\left(1+\mathrm{j}\eta_{\text{pipe}}\right)$, is the complex Young's modulus of the pipe, where E_{pipe}, η_{pipe}, ρ_{pipe} and ν_{pipe} are the Young's modulus, the loss factor, the density and the Poisson's ratio of the pipe-wall respectively. The wave dynamic stiffness matrix for the water inside the pipe is given by

$$\mathbf{K}^{(\text{water})} = \begin{bmatrix} 0 & 0 \\ 0 & -K^{(\text{water})} \end{bmatrix} = \begin{bmatrix} 0 & 0 \\ 0 & \dfrac{-\omega^2 \rho_{\text{water}}}{k^R_{\text{water}}} \dfrac{J_0\left(k^R_{\text{water}} a\right)}{J_0'\left(k^R_{\text{water}} a\right)} \end{bmatrix}, \tag{A.3}$$

where $J_0(\bullet)$ is a Bessel function of the first kind of zero order and ' denotes the derivative with respect to the argument. The term $k^R_{\text{water}} = \sqrt{k^2_{\text{water}} - k^2}$ is the component of the wavenumber in the radial direction, in which $k_{\text{water}} = \omega / c_{\text{water}}$ is the wavenumber for water, where c_{water} is the wave speed in an infinite homogeneous body of water, which is approximately 1500 m/s. At low frequencies, when the acoustic wavelength in water is much greater than the diameter of the pipe $J_0\left(k^R_{\text{water}} a\right) / J_0'\left(k^R_{\text{water}} a\right) \approx -2 / k^R_{\text{water}} a$. Noting that $k^2_{\text{water}} = \omega^2 \rho_{\text{water}} / B_{\text{water}}$, then

$$K^{(\text{water})} \approx \frac{\tilde{K}^{(\text{water})}}{\left(\dfrac{k^2}{k^2_{\text{water}}} - 1 \right)}, \tag{A.4}$$

where $\tilde{K}^{(\text{water})} = 2B_{\text{water}} / a$, in which B_{water} is the bulk modulus and ρ_{water} the density of water. The wave dynamic stiffness matrix for the surrounding medium is given by

$$\mathbf{K}^{(\text{soil})} = G_{\text{soil}} \begin{bmatrix} -\alpha k^R_d & \text{j}\left(2 - \alpha \bar{H}_d\right) k \\ -\text{j}\left(2 - \alpha \bar{H}_d\right) k & \dfrac{2}{a} + \alpha \dfrac{k^R_s}{k^R_d} \bar{H}_s \bar{H}_d k^R_d \end{bmatrix}, \tag{A.5}$$

where $\alpha = \dfrac{k_s^2}{k_d^R k_s^R \bar{H}_s + k^2 \bar{H}_d}$, $\bar{H}_s = H_0\left(k_s^R r\right) \big/ H_0'\left(k_s^R r\right)$ and $\bar{H}_d = H_0\left(k_d^R r\right) \big/ H_0'\left(k_d^R r\right)$, in which $H_0(\bullet)$ is a Hankel function of the second kind of zero order; $k_s^R = \sqrt{k_s^2 - k^2}$, in which $k_s = \omega / c_s$ is the shear wavenumber for the soil, where $c_s = \sqrt{G_{\text{soil}} / \rho_{\text{soil}}}$ is the shear wave speed in the soil in which G_{soil} and ρ_{soil} are the shear modulus an density of the soil respectively; $k_d^R = \sqrt{k_d^2 - k^2}$ in which $k_d = \omega / c_d$ is the compressional wavenumber for the soil, where $c_d = \sqrt{\left(B_{\text{soil}} + 4G_{\text{soil}}/3\right) \big/ \rho_{\text{soil}}}$ is the compressional wave speed in the soil in which B_{soil} is the bulk modulus of the soil.

Noting that $K_{21}^{(\text{pipe})} = -K_{12}^{(\text{pipe})}$ and $K_{21}^{(\text{soil})} = -K_{12}^{(\text{soil})}$, Eq. (A.1), can be rearranged to give an expression for the wavenumber of the predominantly fluid-borne wave, which is given by

$$k = k_{\text{water}} \left(1 + \frac{\tilde{K}^{(\text{water})}}{K^{(\text{pipe})} + K^{(\text{pipe\_soil})} + K^{(\text{soil})}} \right)^{\frac{1}{2}}, \tag{A.6}$$

where $K^{(\text{pipe})} = K_{22}^{(\text{pipe})}$, $K^{(\text{pipe\_soil})} = \dfrac{\left(K_{12}^{(\text{pipe})} + K_{12}^{(\text{soil})}\right)^2}{K_{11}^{(\text{pipe})} + K_{11}^{(\text{soil})}}$ and $K^{(\text{soil})} = K_{22}^{(\text{soil})}$. Note that the wavenumber is a function of the wave dynamic stiffnesses. One of these is related to the water in the pipe $\tilde{K}^{(\text{water})}$, one to the pipe alone $K^{(\text{pipe})}$, one to the soil alone $K^{(\text{soil})}$, and one that is related to the interaction between the pipe and the soil $K^{(\text{pipe\_soil})}$. Note, however, that the wave dynamic stiffnesses in the denominator of Eq. (A.6) are functions of *k*, so Eq. (A.6) is recursive.